

# Co-Precipitation Synthesis of Stable Iron Oxide Nanoparticles with NaOH: New Insights and Continuous Production via Flow Chemistry

Maximilian O. Besenhard,<sup>§</sup> Alec P. LaGrow,<sup>†,‡</sup> Aden Hodzic,<sup>‡</sup> Manfred Kriechbaum,<sup>∇</sup> Luca Panariello,<sup>§</sup> Giorgio Bais,<sup>θ</sup> Katerina Loizou,<sup>§</sup> Spyridon Damilos,<sup>§</sup> M. Margarida Cruz,<sup>δ</sup> Nguyen Thi Kim Thanh,<sup>†,‡,\*</sup> Asterios Gavriilidis<sup>§,\*</sup>

<sup>§</sup> Department of Chemical Engineering, University College London, London, WC1E 7JE, U.K.

<sup>†</sup> Department of Physics and Astronomy, University College London, London, WC1E 6BT, U.K.

<sup>‡</sup> UCL Healthcare Biomagnetic and Nanomaterials Laboratories, University College London, London, W1S 4BS, U.K.

<sup>∇</sup> Institute of Inorganic Chemistry, Graz University of Technology, 8010 Graz, Austria

<sup>‡</sup> Central European Research Infrastructure Consortium, CERIC-ERIC, 34149 Basovizza, Italy

<sup>θ</sup> Elettra Sincrotrone Trieste, Area Science Park 34149 Basovizza, Italy

<sup>δ</sup> Universidade de Lisboa, Faculdade de Ciências, BioISI - Biosystems & Integrative Sciences Institute, 1749-016 Lisboa, Portugal

## Corresponding Authors\*

Corresponding authors' Emails: a.gavriilidis@ucl.ac.uk, ntk.thanh@ucl.ac.uk

**Keywords:** In-situ XRD; In-situ SAXS; Nanoparticle formation kinetics; Co-precipitation; Multistage flow reactor; Continuous production

---

**Abstract:** Co-precipitation is by far the most common synthesis for magnetic iron oxide nanoparticles (IONPs), as cheap and environmentally friendly precursors and simple experimental procedures facilitate IONP production in many labs. Optimising co-precipitation syntheses remains challenging however, as particle formation mechanisms are not well understood. This is partly due to the rapid particle formation (within seconds) providing insufficient time to characterise initial precipitates. To overcome this limitation, a flow chemistry approach has been developed using steady-state operation to “freeze” transient reaction states locally. This allowed for the first time a comprehensive analysis of the early stages of co-precipitation syntheses *via* in-situ Small Angle X-ray Scattering and in-situ synchrotron X-Ray Diffraction. These studies revealed that after mixing the ferrous/ferric chloride precursor with the NaOH base solution, the most magnetic iron oxide phase forms within 5 s, the particle size changes only marginally afterwards, and co-precipitation and agglomeration occur simultaneously. As these agglomerates were too large to achieve colloidal stability *via* subsequent stabiliser addition, co-precipitated IONPs had to be de-agglomerated. This was achieved by adding the appropriate quantity of a citric acid solution which yielded within minutes colloiddally stable IONP solutions around a neutral pH value. The new insights into the particle formation and the novel stabilisation procedure (not requiring any ultra-sonication or washing step) allowed to design a multistage flow reactor to synthesise and stabilise IONPs continuously with a residence time of less than 5 min. This reactor was robust against fouling and produced stable IONP solutions (of ~ 1.5 mg particles per ml) reproducibly *via* fast mixing (< 50 ms) and accurate temperature control at large scale (> 500 ml/h) for low materials cost.

---

## 1. Introduction

Applications involving iron oxide nanoparticles (IONPs) receive considerable attention in fields requiring large quantities such as biomass recovery and agriculture [1–3], and waste water treatment [4]. IONPs with higher quality requirements find applications in catalysis [5,6], batteries [7] and especially biomedicine [8–11], including drug delivery [12,13], magnetic hyperthermia therapy of cancer [10,14,15], and contrast agent for magnetic resonance imaging [16,17]. Their performance depends strongly on the oxide phase, the particle morphology, the size and size distribution, the internal composition (e.g., impurities, and grain boundaries) and the surface chemistry. Therefore, each application requires an optimised synthetic procedure, capable to reproducibly generate the desired IONPs at quantities exceeding lab-scale. The development of such scalable synthesis, and hence large scale production, is still a matter of current research, as indicated from the vast number of studies on IONP syntheses [9,18–20].

Methods using the thermal decomposition of precursors such as ferric acetylacetonates in high-boiling-point organic solvents are known for their potential to synthesise highly monodisperse IONPs of tuneable size [21–23] and examples of scalable synthesis exist [24]. The relatively long reaction times (of the order of an hour) allow for comprehensive analysis during the synthesis, which led to an advanced understanding of particle formation mechanism during thermal decomposition syntheses [25–27]. However, these syntheses are labour and cost-intensive (especially for large-scale production) as they necessitate high temperatures (usually > 250 °C) and costly chemicals. Furthermore, thermal decomposition syntheses require post-processing steps, such as purification and phase transfer, usually after a time-consuming ligand exchange step, if IONPs need to be dispersed in aqueous solutions. This is the case for most biomedical applications, where also the chemicals commonly used for thermal decomposition face severe challenges regarding the stringent control by regulatory bodies. Therefore, water-based syntheses are more desirable.

This is one of the reasons why the most commonly used synthesis of IONPs is the co-precipitation of iron salts in aqueous solutions, *i.e.*, the simultaneous precipitation of ferrous and ferric ions initiated by the addition of a base. Other reasons for the popularity of the co-precipitation synthesis are the cheap chemicals, and simple experimental procedures at moderate temperatures (< 100 °C) without toxic educts or by-products. However, co-precipitation syntheses are known to yield particles of a relatively low magnetisation and high polydispersity due to variations in IONP core sizes and the presence of agglomerates. These agglomerates pose new challenges to stabilisation, and the IONPs' utilisation. For example, the IONP distribution in the body tissue depends strongly on the core and agglomerate size. Variations in core size are expected to originate from simultaneous nucleation and growth of particles and the occurrence of intermediate phases before or during the formation of the desired magnetic phases, *i.e.*, magnetite (Fe<sub>3</sub>O<sub>4</sub>) or maghemite ( $\gamma$ -Fe<sub>2</sub>O<sub>3</sub>) [28,29]. The particle formation mechanism remains still a matter of discussion and is expected to diverge depending on the synthesis conditions (precursors used and their concentration, temperature, pH, sequence of reagent and stabiliser addition, etc.) [30–33]. Only some recent studies were able to provide some insights into the particle formation mechanisms during co-precipitation, as described below.

Ahn *et al.* performed XRD and TEM studies on samples taken every few minutes during the dropwise addition or one hour after the rapid addition of an ammonium hydroxide (NH<sub>4</sub>OH) base solution to a 1:2 mol ratio ferric to ferrous chloride precursor solution. Akaganeite ( $\beta$ -FeO(OH)) and goethite ( $\alpha$ -FeO(OH)) were identified as intermediate phases when increasing the pH slowly, *i.e.*, *via* the dropwise addition of the base solution. Other phases including ferrous hydroxides and lepidocrocite were reported to form as intermediates or by-products

before the formation of magnetite/maghemite (and goethite as minor phase for  $\text{NH}_4\text{OH}$  to Fe-ion (ferric and ferrous) ratios  $< 2.6$ , yielding a pH of 5, and major phase for lower pH values) when adding the base abruptly [28]. The different formation pathway and the formation of lepidocrocite ( $\gamma\text{-FeO(OH)}$ ) in the case of abrupt base addition were proposed to originate from local variations in pH due to insufficient mixing, which altered the reaction rate and pH at which precipitation occurred. This highlights the importance of rapid and controlled mixing for reproducible co-precipitation syntheses. Baumgartner *et al.* presented cryo-TEM studies during the slow addition of an iron chloride solution to a dilute NaOH solution while keeping the pH constant using titration set-up adding NaOH. Their results indicate a colloidal growth process of magnetite after the formation of primary initial hydroxide particles [29]. Studies using a weaker base, *i.e.*, sodium bicarbonate, to slow down the precipitation process, showed differences in the particle formation pathway depending on the pH and temperature [34]. Syntheses of 60 min reaction time yielded magnetite as the dominant phase if  $\text{pH} \geq 8$  and goethite, accompanied with siderite ( $\text{Fe(CO}_3\text{)}$ ), at lower pH values when performed at room temperature. Taking samples for subsequent XRD studies every minute after the dropwise base addition showed that at pH 9, goethite is formed as an intermediate phase which later transforms into magnetite. However, at temperatures above  $50\text{ }^\circ\text{C}$  magnetite was formed quicker, *i.e.*, became the dominant phase in the first sample taken after mixing. Time-resolved XRD studies demonstrated that at these temperatures magnetite is formed minutes after mixing (a semi-batch set-up allowed for fast mixing) and without the occurrence of goethite if the exposure to air is minimised during the initial phase of the reaction. Instead, an iron hydroxide carbonate ( $\text{Fe}_6(\text{OH})_{12}\text{CO}_3$ ) and a poorly crystalline ferrihydrite phase ( $\text{Fe}_{10}\text{O}_{14}(\text{OH})_2$ ) were identified as intermediates which were then simultaneously consumed during the nucleation and growth of magnetite NPs [35].

Currently, there is no common agreement of the particle formation mechanism, which is most likely associated with variations in the synthesis procedure but also with rapid particle formation ( $\ll 1\text{ s}$ ) after the addition of the base. Such rapid phase changes complicate the IONP characterisation and affect the reproducibility of process conditions. Fluctuations in mixing time (and associated local fluctuations in pH, and concentration) are expected to alter the intermediate oxide phases and, hence, the final IONP properties, as well as the nucleation kinetics. The importance of mixing conditions for the IONP size distribution (with smaller but more monodisperse particles obtained with faster mixing) is well documented [36,37].

Evidently, co-precipitation syntheses are sensitive to the reaction conditions, which complicates their optimisation without compromising scalability. Flow reactors offer a solution to this obstacle by providing alternatives routes to execute syntheses at highly controlled process conditions, while providing options for large-scale production by long operation times. In addition, flow reactors enable experimental procedures to study rapid nanoparticle formation mechanisms even at the early reaction stages (which are most important in the case of co-precipitation) *via* steady-state operations, by locally “freezing” reaction states and thus making them accessible to characterisation techniques that require measurement times larger than the timescale of particle formation dynamics [38–40].

Although the potential of flow reactors for continuous co-precipitation has been demonstrated [41–44], reactor optimisation is hardly possible due to incomplete knowledge on particle formation kinetics (likewise to batch procedures). Therefore, this work presents: i) The utilisation of flow reactors to gain insights into the particle formation mechanism from the first few seconds of a co-precipitation synthesis of IONPs using sodium hydroxide *via* in-situ synchrotron X-ray diffraction (XRD) and small-angle X-ray scattering (SAXS) studies. ii) The stabilisation of IONPs without the requirement of any post processing steps, such as ultra-sonication or washing steps, which was achieved by citric

acid addition to just-precipitated IONPs. The timescale of this stabilisation process (as well as the stages of agglomeration before stabilisation) was monitored *via* SAXS. The kinetic information obtained on IONP formation and the stabilisation procedure developed, made a fully continuous co-precipitation synthesis possible. iii) The development of a multistage flow reactor providing well-controlled temperature and mixing conditions for the precipitation and subsequent stabilisation step. This optimised flow reactor made it possible to continuously synthesise highly stable and monodisperse IONPs with reproducible particle characteristics.

## 2. Materials and methods

### 2.1. Flow reactor for in-situ XRD and SAXS studies

The flow reactor used for the in-situ XRD studies was heated to the reaction temperature of 60 °C in a water bath and fed by a syringe pump (Legato210, KD Scientific Inc., USA) equipped with two 100 ml gas tight syringes (SGE syringes - TRAJAN, Australia). The syringes containing the precursor and base solutions were followed by 5 m long PTFE tubing with an inner diameter (I.D.) of 1 mm to get both solutions to the reaction temperature before mixing (see Figure S1 for the simulated temperature profile in this tubing) [45]. Mixing occurred in a ETFE T-mixer with an I.D. of 0.51 mm (if not mentioned otherwise) hereinafter referred to as standard T-mixer. This simple mixing element allowed for mixing times < 50 ms for aqueous solutions at 60 °C and the used flow rate of 5 ml/min for both solutions, *i.e.*, 2 x 5 = 10 ml/min in total at Reynolds number,  $Re = 893$ , as determined *via* the Villermaux-Dushman protocol [35]. For the in-situ synchrotron XRD studies, the T-mixer outlet was connected to an XRD flow cell which was placed within the synchrotron beamline. The T-mixer outlet was connected to the flow cell either directly or through coaxial flow inverters (CFI) to increase the residence/reaction time at which a pattern was recorded. The CFI to increase the residence time by 30 s consisted of 6.4 m PTFE tubing with an I.D. of 1 mm coiled at a curvature of  $2.22\text{ cm}^{-1}$ , see Figure S3d. CFIs for longer residence times were made of PTFE tubing with an I.D. of 1.51 mm coiled at a curvature of  $0.9\text{ cm}^{-1}$ . For all CFIs, the flow was inverted every four turns. Synchrotron studies were performed at the X-ray diffraction beamline (XRD1) of the Elettra Synchrotron (Trieste, Italy) with a monochromatic wavelength of 0.1 nm (12.4 keV) passing through the quartz capillary of the flow cell. Since the precipitated solutions were of a low solid mass concentration (< 2.5 mg Fe in the form of magnetic nanoparticles per ml solution), patterns were recorded for 10 min to guarantee satisfactory signal quality. Further details of the synchrotron settings, the flow reactor(s) and CFI(s) and the XRD flow cell, as well as data analysis including the background subtraction are provided in the Supporting Information, SI 2.2. For the in-situ SAXS studies, the T-mixer was connected to the flow cell of a SAXSess system (Anton Paar, Austria). Further details of the SAXS settings, the flow cell, as well as data analysis are provided in the Supporting Information, SI 2.3.

### 2.2. Chemicals and synthesis

Precursor solution: 0.1 M Fe ion solution, prepared by dissolving ferrous and ferric chlorides in a 1:2  $\text{FeCl}_2 \cdot 4\text{H}_2\text{O}$ :  $\text{FeCl}_3 \cdot 6\text{H}_2\text{O}$  molar ratio in deionised (DI) water (resistivity  $\geq 15\text{ M}\Omega/\text{cm}$ ,  $\text{pH}_{\text{prec}} = 1.8$ ). Base solution: DI water mixed with 2 M NaOH in a 10:4 volumetric ratio (0.57 M NaOH). Neutralisation solution: 0.316 M citric acid solution,  $\text{pH}_{\text{neutr}} = 1.8$ . All chemicals, the provider and lot numbers are listed in table S1.

IONPs were co-precipitated by mixing the precursor and base solution of the (standard) concentrations stated above (if not mentioned otherwise). Mixing was performed at a reaction temperature of 60 °C for all syntheses. The sequence of neutralisation solution addition and the added quantity varied with the experiment.

### 2.3. Nanoparticle characterisation

The concentration of Fe in the form of magnetic nanoparticles, which is referred to as solid mass concentration ( $\text{mg}_{\text{Fe IONP}}/\text{ml}_{\text{sol}}$ ), and the associated precursor conversion ( $\% \text{Fe} = \text{mg}_{\text{Fe IONP}}/\text{mg}_{\text{Fe sol}} \cdot 100$ ) were determined by microwave plasma atomic emission spectroscopy (MP-AES) using a 4210 MP-AES system (Agilent, USA). Solutions for MP-AES measurements were prepared by washing the sample solutions twice (addition of ethanol, magnetic decantation and re-dispersion in deionised water) before drying in air and dissolution in aqua regia (3:1 volumetric ratio of HCl:HNO<sub>3</sub>). Dynamic light scattering (DLS) studies were performed using a DelsaMax-Pro (Beckman Coulter, USA) at 22 °C. For the determination of the hydrodynamic diameter, the samples (as synthesised) were diluted with DI water till the measured size plateaued (typically at volumetric ratios > 1:4 of sample solution : DI water). Transmission electron microscope (TEM) images were captured using a JEOL 1200 EX microscope with a 120 kV acceleration voltage. Samples were prepared using carbon-coated copper grids and using washed samples only, if not specified otherwise. Particle sizes were obtained using ImageJ, measuring at least 100 particles by fitting a polygon around the particles' edges to determine their area. Reported diameters refer to the (average) circle of equal projection area. Offline SAXS measurements were performed with a Ganesha SAXSlab (Xenocs, France) using a point focus X-ray source and a 2D detector for collection times of at least 1 h. All SAXS curves were recorded the next day after synthesis. The magnetic properties were characterised by hysteresis curves up to 5.5 T and zero-field and field cooled measurements using a magnetic property measurement system (MPMS, Quantum Design, USA) superconducting quantum interference device (SQUID) magnetometer.

## 3. Results and discussion

### 3.1. Synchrotron XRD studies

The possibility to “freeze” reaction states by steady-state operation of a flow reactor facilitated XRD and SAXS analysis (next section) of intermediate states during the co-precipitation synthesis with NaOH. To uncover which phase(s) are formed immediately after mixing and unravel the kinetics of magnetite formation, a flow reactor set-up in combination with a flow cell for XRD was used as described in section 2.1. As sketched in Figure 1a, using a minimum length of 1 m PTFE tubing (internal diameter I.D. = 1 mm) to connect the T-mixer in the water bath with the flow cell made it possible to record an XRD pattern only 5 s after mixing. Using coiled flow inverters with different lengths allowed to record patterns for residence times between 35 and 160 s.

The XRD patterns obtained (see Figure 1b) show that even 5 s after mixing, magnetite was the only evident crystalline phase. It must be noted that a clear differentiation between magnetite and maghemite is not possible based on XRD patterns and references to magnetite should be considered as references to magnetite/maghemite mixtures. Within the next 50 s (here referring to the residence time), the intensity of the magnetite peaks increased by ~ 20% compared with intensities at 5 s, increasing only marginally within the next minutes (~ 8% after 100 s and 10% after 160 s; both compared to 50 s). Furthermore, all XRD patterns showed no sign of any (crystalline) intermediate phases, *i.e.*, phases other than magnetite. This indicates that solid phase formation approaches completion within minutes and shows the absence of

crystalline intermediate phases just 5 s after mixing. These results differ from previous studies on the particle formation mechanism [28,29,35], commonly reporting the occurrence of intermediate phases before the transition to magnetite occurring within minutes or hours. However, these previous studies were limited to co-precipitation synthesis at low pH with a slow addition of the base solution to allow timely sampling. The immediate formation of magnetite was speculated for a 1:2 ratio of ferrous and ferric ions and relatively high pH [30].

In order to study the effect of mixing conditions and the presence of dextran as a stabiliser, additional synchrotron XRD studies were performed using an on-line semi-batch set-up, recycling just-precipitated (exiting the T-mixer) IONP solutions through the XRD flow cell *via* a peristaltic pump, as described in SI 2.2.2. The XRD pattern of solutions mixed at Reynolds numbers (Re) of 359, 893 and 3037 (using the same flow reactor but different T-mixers with I.D. of 1.27, 0.51, and 0.15 mm) did not show a clear difference in their XRD patterns, see Figure S8. Furthermore, there was no apparent difference between the first recorded pattern (3 min after mixing for these on-line studies) and the last pattern 33 min after mixing. The presence of a stabiliser (dextran which was premixed into the base solution) during mixing, however, did alter the XRD pattern significantly, see Figure S9. The diffraction peaks became significantly broader and of a lower intensity, indicating the formation of smaller particles. This is in agreement with previous studies reporting inhibited growth of IONPs if co-precipitation occurs in the presence of dextran yielding sizes  $\leq 6$  nm [46,47].

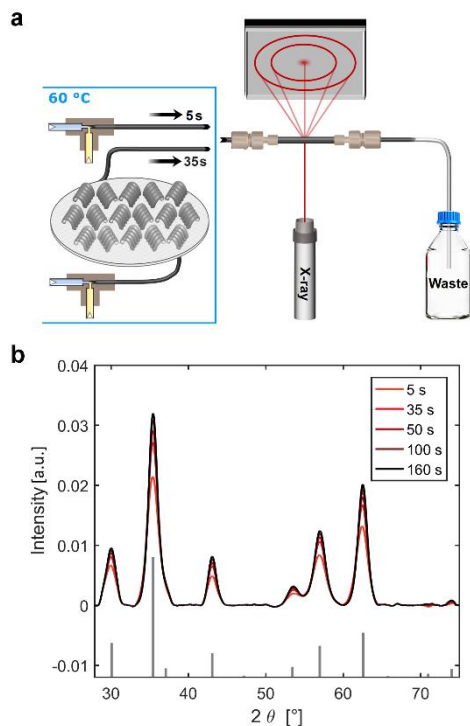


**Figure 1:** (a) Schematic of set-up for in-situ XRD studies, “freezing” the temporal reaction states after mixing the precursor and base solutions by adjusting the tube length before the flow cell from 5 s (minimum residence time between T-mixer and flow cell) to 35 s - 160 s using a coiled flow inverter (here sketched for a residence time of 35 s). (b) XRD pattern during the first 160 s after mixing the precursor and base solutions. The bars at the bottom show the peak positions and relative intensities of magnetite. Scattering angles were rescaled to the Cu K- $\alpha_1$  radiation with  $\lambda = 0.154$  nm.

### 3.2. SAXS studies

To investigate the morphology of just-precipitated IONPs, in-situ SAXS studies were performed. Therefore, the outlet of the flow reactor (as used for the in-situ synchrotron XRD studies), was coupled to the flow cell of a SAXS system, see section 2.1 for details. The SAXS curves recorded in-situ 5 s after mixing the precursor and base solutions (base concentrations of 0.5 and 1 M NaOH were used, *i.e.*, a lower and a higher concentration than the standard base solution) revealed a strong (linear) intensity increase towards small  $q$  values in the  $\log(\text{Intensity})$  vs.  $\log(q)$  plot which is a characteristic of agglomerated structures [48], see Figure S10. This indicates that particle agglomeration happens simultaneously with particle formation and not afterwards.

For a better understanding how mixing affects the morphology of just-precipitated IONPs, the mixing conditions were altered by using different T-mixers (the same parts as for the synchrotron XRD studies; and the standard NaOH concentration of 0.57 M). Additionally, a batch study was performed for comparison. The experimental details and the analysis of SAXS curves obtained for different mixing conditions (see Figure S11) are described in SI 3.2. This analysis included the surface to volume ratio summarised in Table S3. It was observed that the use of the T-mixer with the smallest I.D. yielded the highest surface area ( $Re = 3037$ ,  $90.1 \text{ m}^2/\text{cm}^3$ ) followed by the T-mixers with larger I.D.s ( $Re = 893$ ,  $87.9 \text{ m}^2/\text{cm}^3$  – the standard T-mixer;  $Re = 359$ ,  $83.9 \text{ m}^2/\text{cm}^3$ ). Despite vigorous stirring, particles synthesised in batch exhibited a significantly lower surface to volume ratio ( $69.4 \text{ m}^2/\text{cm}^3$ ).

The in-situ SAXS analysis revealed that the just-precipitated IONPs are highly agglomerated. Hence, colloiddally stable IONP solutions cannot simply be achieved through the addition of a stabiliser after mixing the precursor and base solutions. Even though the attachment of ligands for electrostatic or steric stabilisation on the IONPs surface should reduce further agglomeration, the agglomerates formed during precipitation (*i.e.*, within seconds after mixing) are already too large to avoid sedimentation and are likely to interact magnetically. Therefore, the initially formed agglomerates need to be “de-agglomerated”. Ultra-sonication is probably the most common method to break up agglomerates and is therefore part of most stabilisation procedures for co-precipitated IONPs [18,49]. However, ultra-sonication lacks control, scalability, and might not be sufficient to achieve complete de-agglomeration. Furthermore, its translation into flow is not trivial and would require additional process steps. Therefore, a different approach was used for stabilisation (and de-agglomeration) of the IONPs without any ultra-sonication, washing or other intermediate processing steps. This was achieved *via* the addition of a citric acid solution (herein referred to as neutralisation solution) fed to the already precipitated IONP solution. The purpose of the neutralisation solution was not only to introduce stabilisers and drop the pH to allow them to attach to the particle surface (the current counter ions such as hydroxyl groups, dominating at high pH values, need to be replaced), but also to de-agglomerate the highly agglomerated structures formed during precipitation.

To monitor the morphological changes of IONPs after the addition of the neutralisation solution, at-line SAXS studies were performed using a semi-batch set-up described in SI 2.3.2. As sketched in Figure S7, the just-precipitated IONP solution exiting the (standard) T-mixer was collected in an aging vessel for 2 min (20 ml in total). This vessel was magnetically stirred and kept at the reaction temperature of 60 °C. The neutralisation solution was added into this aging vessel *via* a pipette ( $2.1 \text{ ml}_{\text{neutr}}$  per  $10 \text{ ml}_{\text{IONP}}$  solution) 100 s after the collection of the solution finished. Samples for SAXS analysis were then withdrawn manually with a syringe at different times. The in-situ SAXS curve of

just-precipitated IONP solutions (5 s after mixing the precursor and base solutions with the standard T-mixer) and the at-line SAXS curves of samples withdrawn after the neutralisation solution was added, are shown in Figure 2.

The SAXS curve recorded immediately ( $\sim 20$  s) after the addition of the neutralisation solution showed an immediate change in particle morphology. The next samples taken at 3 and 10 min (after adding the neutralisation solution) showed that IONPs continued de-agglomerating, as evident from the Guinier region in which the curve became more linear over time. This is as expected for non-agglomerated particles in a  $\ln(\text{Intensity})$  vs.  $q^2$  plot [38,50]. Beyond 10 min after neutralisation, the SAXS curve changed only marginally indicating the end of morphological changes (see Figure 2), hence, the completion of de-agglomeration. If no neutralisation solution was added, the at-line SAXS curves of the just-precipitated solution collected in the aging vessel (withdrawn 5 and 10 min after the solution collection finished, data not shown), showed no change compared to the in-situ curve recorded 5 s after mixing.

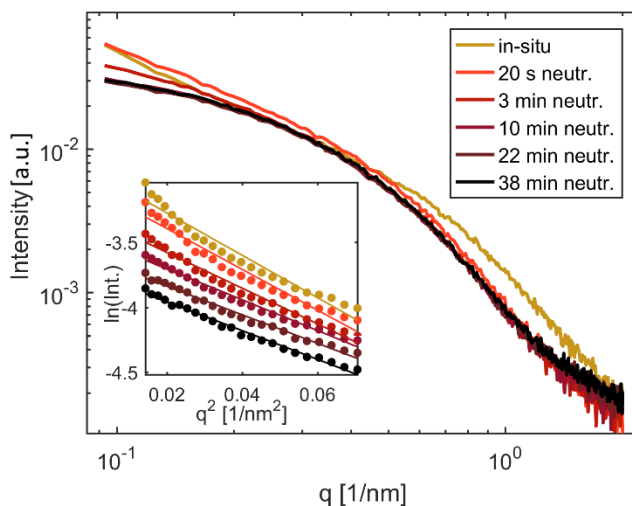


**Figure 2:** SAXS curves of the IONPs obtained 5 s after mixing the precursor and base solutions (measured in-situ) and 20 s - 38 min after the addition of neutralisation solution (measured at-line). The inset shows the Guinier plots (plotted with an offset for easier comparison of the linear fit quality).

### 3.3. Continuous production of stable IONPs via a flow reactor

Based on the insights into particle formation dynamics gained from in-situ XRD and SAXS studies and the de-agglomeration dynamics after the addition of the citric acid solution (= neutralisation solution) gained from at-line SAXS studies, a flow reactor for the continuous co-precipitation synthesis of IONPs and subsequent stabilisation was developed. A schematic of this multistage flow reactor is shown in Figure 3. It consisted of the mixing elements, as described in section 2.1. (1<sup>st</sup> water bath in Figure 3) and was operated likewise, *i.e.*, at reaction temperature of 60 °C and precursor and base solution flow rates of 5 ml/min each (iron precursor and sodium hydroxide concentrations provided in Materials and Methods). The standard T-mixer with an I.D. of 0.51 mm ( $Re = 893$ ) was retained due to the low pressure drop compared to the tested T-mixer with an I.D. of 0.15 mm ( $Re = 3037$ ), since it was shown to have insignificant effect on the just-precipitated IONPs by the XRD (Figure S8) and SAXS (Figure S11) studies. The mixing time of  $< 50$  ms was still faster than what is possible in standard

lab-scale batch reactors, even at vigorous stirring, hence, minimising spatio-temporal pH fluctuations and facilitating precipitation at homogeneous conditions. It is worth noting that the simple geometry of the T-mixers, *i.e.*, no edges or grooves resulting to dead zones was essential to avoid fouling in combination with the relatively high flow rates. The importance of sufficient shear force to avoid crustation and plugging was shown before for IONP synthesis [51]. The T-mixer used plugged occasionally during operation at lower flow rates (1 ml/min was tested). The PTFE tubing showed no indications of fouling which was attributed to the highly negative zeta potential values of PTFE tubing in alkaline solutions ( $< -40$  mV at  $\text{pH} > 9$ ) [52].

For the continuous flow reactor, the mixing step was followed by an aging stage (2<sup>nd</sup> water bath in Figure 3), implemented by a CFI consisting of three layers which the just-precipitated IONPs reached  $\sim 5$  s after mixing. The first two with a mean residence time of 50 s each and the third with mean residence time of 60 s (total residence time after mixing 160 s). Since the synchrotron XRD studies indicated that particle formation is almost complete after 100 s, the neutralisation solution was fed after the first two layers of the CFI using a second T-mixer (I.D. = 0.51 mm) with its outlet connected to the third CFI layer of the aging stage. All CFI layers were immersed in a heated water bath to maintain the reaction temperature. Further experiments on the timing of the neutralisation step (see SI 3.3), showed that the neutralisation solution should be added within 30 min after mixing to ensure efficient de-agglomeration. A detailed description of the flow reactor developed is provided in SI 2.1.

The mean residence time in the reactor (calculated based on the total flow rate and the reactor volume) was less than 5 min, accounting for the average time the solution spent between exiting the syringes and arrival in the collection vial. Since SAXS studies showed that de-agglomeration takes up to 10 min, see Figure 2, and the residence time of the IONP solution in the flow reactor after the addition of neutralisation solution was  $\sim 60$  s, the vials collecting the IONP solution exiting the reactor were changed every 3 - 5 min (collecting 36.3 - 60.5 ml for a neutralisation solution feed rate of 2.1 ml<sub>neutr</sub>/min). This minimised the collection of IONP solutions of different de-agglomeration states. Typical operation times of the reactor where  $\sim 20$  min, producing  $\sim 200$  ml of IONP solution, and were limited only by the volume of the syringes used. As indicated by experiments where the syringes were recharged several times without intermediate reactor cleaning (see large-scale production studies in SI 3.8), longer operation times can be achieved using any continuously operating pumps providing delivery pressures  $> 2$  bar.

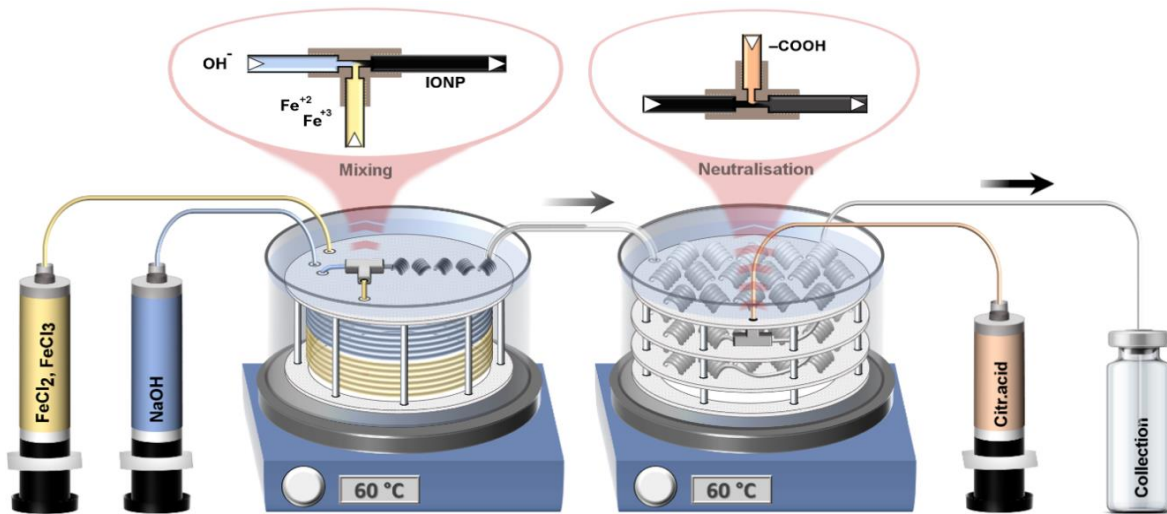


**Figure 3:** Schematic of the multistage flow reactor for the continuous production of stable IONPs using a co-precipitation synthesis followed by a stabilisation step. The reactor allowed preheating the precursor and base solutions and then mixing in a T-mixer and a subsequent coiled flow inverter (in the first water bath), as well as subsequent aging in a three-layer coiled flow inverter where a citric acid solution was added (= neutralisation) via a second T-mixer (in the second water bath).

The right quantity of neutralisation solution was the key to a successful synthesis of stable IONP solutions. Neutralisation to IONP solution ratios of less than 1.7 ml<sub>neutr</sub> solution per 10 ml<sub>IONP</sub> solution (*i.e.*, for neutralisation solution flow rates < 1.7 ml<sub>neutr</sub>/min) resulted in unstable solutions with particles sedimenting within 30 min after collection. Neutralisation to IONP solution ratios exceeding 2.5 ml<sub>neutr</sub> solution per 10 ml<sub>IONP</sub> solution (*i.e.*, for neutralisation solution flow rates > 2.5 ml<sub>neutr</sub>/min) resulted in the complete dissolution of particles, see Figure 4. The pH values of the synthesised IONP solutions show the buffering effect of the IONPs, as the pH dropped rapidly with the addition of neutralisation solution until reaching a plateau where the solutions became stable. After the complete dissolution of IONPs, the pH value then continued to drop with increasing neutralising solution feed rates. Due to this buffering effect, the solid mass concentration ( $C_{\text{solid mass mg}_{\text{Fe IONP}}/\text{ml}_{\text{sol}}}$ ) and hence the precursor conversion ( $X_{\text{Fe}} \%$ ) decreased with the amount of neutralisation solution added. For non-stabilised samples, *i.e.*, neutralisation solution flow rates of 0 ml<sub>neutr</sub>/min, the solid mass concentration was 2.1 mg<sub>Fe IONP</sub>/ml<sub>sol</sub> with a precursor conversion of 88%. For neutralisation solution flow rates of 1.7-2.5 ml<sub>neutr</sub>/min, the precursor conversion was 20-70% (see Table 1). Despite this drop in solid mass concentration with neutralisation solution flow rate, the IONPs core size changed only by a small margin. This was attributed to the fact that the particle volume scales with diameter to the power of three, but also to preferential dissolution of the smallest (usually less ordered/crystalline) particles.

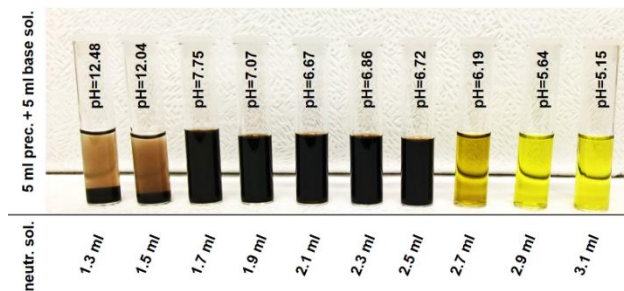


**Figure 4:** Synthesis products obtained from the multistage flow reactor for various feed ratios of neutralisation solution, *i.e.*, 1.3-3.1 ml<sub>neutr</sub> per 10 ml<sub>IONPs</sub> (from 5 ml precursor solution + 5 ml base solution). The corresponding pH of the solution obtained is also indicated.

The stable solutions were of a neutral pH value, *i.e.*, between 7.5 and 6.5. Since the isoelectric point of pristine IONPs is in this range, colloidal stability could not have been achieved without successful stabilisation. When dextran was added to the neutralisation solution (*i.e.*, citric acid and dextran), the stabilisation could be achieved for the same neutralisation to IONP solution ratios, but a change in the properties of synthesised IONPs compared to those stabilised using only citric acid was not observed, see SI 3.5. Stable IONP solutions could also be synthesised using a neutralisation solution containing HCl instead of citric acid (results not shown). However, stabilisation (neither sedimentation nor complete dissolution of particles) was obtained at a pH value between 2 and 3 and the onset of sedimentation was observed after 1-2 weeks.

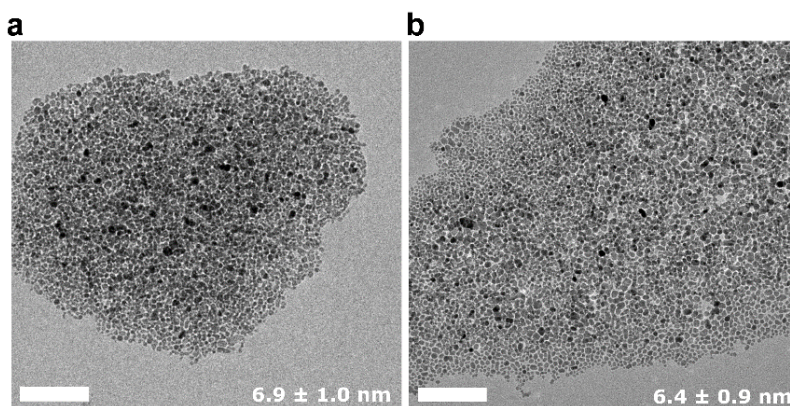


**Figure 5:** TEM images of IONPs obtained from the multistage flow reactor with citric acid neutralisation solution feed rates of: (a) 2.1 ml<sub>neutr</sub>/min and (b) 2.5 ml<sub>neutr</sub>/min (10 ml/min IONP solution). The scale bar is 100 nm in both images. Additional TEM images for these feed rates (from which the diameters were obtained) and 1.9 and 2.3 ml<sub>neutr</sub>/min are shown in Figure S13.

The successful de-agglomeration and stabilisation agrees with the TEM studies showing clear spacing between the IONPs, see Figure 5 and Figure S13. Successful de-agglomeration was also demonstrated by DLS, see Table 1, where the hydrodynamic diameters (indicating the apparent size of the solvated IONPs) were ~ 20 nm for solutions synthesised with neutralisation solution feed rates  $\geq 2.1$  ml<sub>neutr</sub>/min.

For lower neutralisation solution feed rates, the hydrodynamic diameters increased and below feed rates of 1.9 ml<sub>neutr</sub>/min it reached a size that caused the IONPs to sediment, inhibiting the characterisation *via* DLS. This de-agglomeration with increasing neutralisation solution feed rate is also consistent with the (offline) SAXS results in Figure 6 and Table 1, showing a continuous decrease of the radius of gyration ( $R_g$ ) with the neutralisation solution feed rate. It should be noted that all SAXS and DLS analyses were performed on the as-synthesised

samples, *i.e.*, IONP solutions collected directly from the reactor outlet without any washing or ultra-sonication preceding the analysis, and measurements were performed one day after synthesis (if not mentioned otherwise).

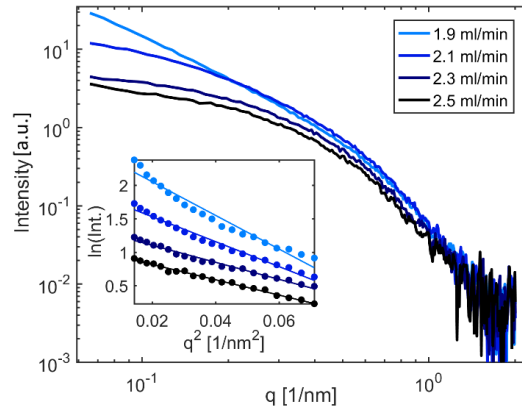


**Figure 6:** SAXS curves of stable IONP solutions obtained from the multistage flow reactor with neutralisation solution feed rates of 1.9-2.5 ml<sub>neutr</sub>/min (10 ml/min IONP solution). The inset shows the Guinier plots (plotted with an offset for easier comparison of the linear fit quality).

When operating at the appropriate neutralisation solution feed rates, IONP solutions exiting the reactor after only 5 min, were highly stable (no signs of sedimentation after several months), without any washing or sonication step post synthesis, *i.e.*, as collected from the reactor outlet.

Even in the case of the lowest precursor conversion, this reproducible synthesis procedure (see demonstration of reproducibility in SI 3.8) remains highly cost-effective due to the usage of low-cost chemicals (< 5 £/g IONPs, see estimation of cost of chemicals in SI 3.9). Although the as-synthesised IONP solution showed no apparent changes for time spans of more than one year and the hydrodynamic diameter showed no significant changes over days (see SI 3.3) and weeks after the synthesis (results not shown), it is recommended to wash the IONPs for long term storage (either as dried particles or in DI water) as described in section 2.3. The washed and dried IONPs were of excellent colloidal stability after redispersion in DI water and the hydrodynamic diameter (measured before washing and drying, and after redispersion) remained unchanged.

**Table 1.** Characterisation summary of synthesised IONP solutions including pH, solid mass concentration,  $C_{\text{solid mass}}$  and precursor conversion,  $X_{\text{Fe}}$  (obtained by MP-AES), particle diameter  $D_{\text{TEM}}$  (obtained by TEM), particle radius of gyration  $R_{\text{g SAXS}}$  and the associated diameter assuming spherical particles  $D_{\text{SAXS}} = 2 R_{\text{g SAXS}} \sqrt{5/3}$  (obtained by SAXS), and hydrodynamic diameter  $D_{\text{h}}$  (obtained by DLS).

Feed rate ratio [ml <sub>neutr</sub> /ml <sub>IONP</sub> ]	pH [-]	$C_{\text{solid mass}}$ [mg <sub>Fe IONP</sub> /ml <sub>sol.</sub> ]	$X_{\text{Fe}}$ [%]	$D_{\text{TEM}}$ [nm]	$R_{\text{g SAXS}}$ [nm]	$D_{\text{SAXS}}$ [nm]	$D_{\text{h}}$ [nm]
$\leq 1.5/10$	> 12	*		No colloidal stability, no further analysis possible			
1.7/10	7.76	1.65	70	Insufficient colloidal stability, signs of sedimentation			
1.9/10	7.07	1.40	57	$7.0 \pm 1.2$	5.6	14.5	39.2
2.1/10	6.87	1.10	45	$6.9 \pm 1.0$	5.3	13.7	19.1
2.3/10	6.86	0.77	32	$7.5 \pm 1.5$	4.9	12.7	19.0
2.5/10	6.72	0.48	20	$6.4 \pm 0.9$	4.8	12.4	23.1
$\geq 2.7/10$	< 6.2			Complete dissolution of particles, no further analysis possible			
* For the non-stabilised sample, <i>i.e.</i> , ml <sub>neutr</sub> /ml <sub>IONP</sub> = 0, $C_{\text{solid mass}} = 2.1$ mg <sub>Fe IONP</sub> /ml <sub>sol.</sub> and $X_{\text{Fe}} = 88$ %							

SQUID analysis confirmed that both the non-stabilised samples and the stabilised IONPs were superparamagnetic (see complete discussion of magnetic characterisation in SI 3.7). The hysteresis curves (see Figure 7a for 0 and 2.1 ml<sub>neutr</sub>/min and Figure S17a for 0, 1.9 and 2.1 ml<sub>neutr</sub>/min) proved that non-stabilised and stabilised samples IONPs were superparamagnetic with coercivities < 1 mT. The saturation mass magnetisations of 62 and 59 Am<sup>2</sup> per kg of washed and dried IONPs (*i.e.*, 62 and 59 emu/g<sub>sample</sub>) were comparable to co-precipitated maghemite nanoparticles of less than 10 nm (to which the samples most likely transformed after handling in air over a prolonged period), where the different spin ordering at the surface layer reduces the particle average magnetic moment. The zero-field and field cooled measurements (see Figure 7b for 2.1 ml<sub>neutr</sub>/min and Figure S17b for 0, 1.9 and 2.1 ml<sub>neutr</sub>/min) showed blocking temperatures of ~ 170 K for stabilised IONPs and ~ 220 K for non-stabilised IONPs. Since TEM analysis revealed the core sizes were comparable for these samples (see Table 1), the higher blocking temperature of the non-stabilised sample is evidence of stronger magnetic interactions of the IONPs in the completely agglomerated structures.

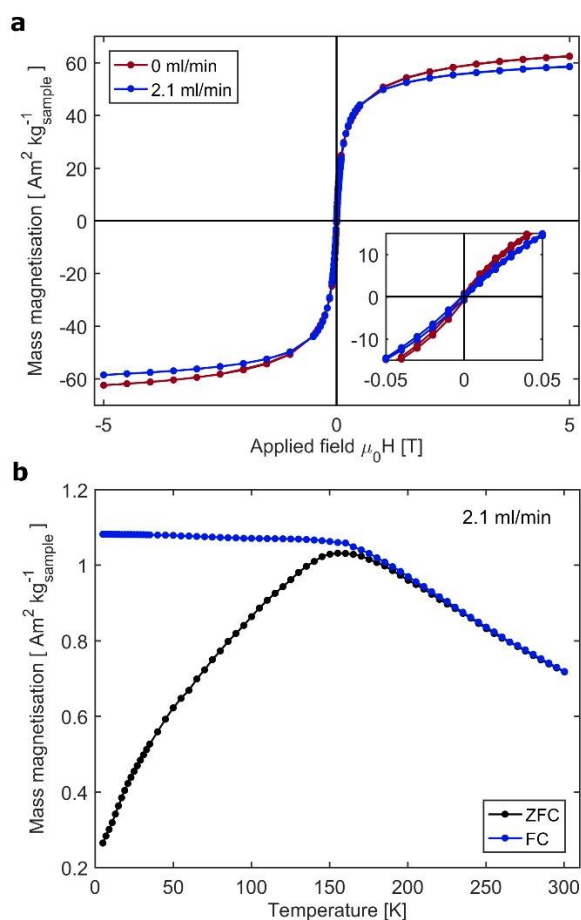


**Figure 7:** (a) Hysteresis curves of non-stabilised (neutralisation solution flow rate of 0 ml<sub>neutr</sub>/min) and stabilised (neutralisation solution flow rates of 2.1 ml<sub>neutr</sub>/min) IONPs. (b) Corresponding zero-field-cooling (ZFC) and field-cooling (FC) curves recorded at 2 mT.

### 3.4. Summary of IONP formation and stabilisation mechanism

Additional TEM studies were performed for IONPs obtained using a semi-batch set-up (similar to that shown in Figure S7, *i.e.*, sampling from the aging vessel but without addition of neutralisation solution) directly onto a TEM grid on a filter. These images (see Figure 8a), show an increase in particle size from about 5.7 to 7.6 nm (analysing single particles, not agglomerates) within the first two minutes after mixing the precursor and base solutions. Beyond 2 min after initial precipitation no further growth was observed (TEM images from samples collected after 3 min not shown), which is in good agreement with the in-situ XRD studies.

Based on these results on the initial particle precipitation and growth mechanism as well as the de-agglomeration and stabilisation timescale revealed by time-resolved SAXS studies, the IONP particle formation mechanism during the continuous co-precipitation synthesis with citric acid stabilisation is summarised in Figure 8b. The co-precipitation synthesis yielded magnetite NPs 5 s after mixing of the precursor and base solution. These just-precipitated IONPs were highly agglomerated and grew only slightly from 5.5 nm to 7.6 nm during the next few minutes. The addition of a solution containing citric acid (the neutralisation solution) resulted in the partial dissolution of the formed IONPs. This partial dissolution yielded slightly smaller, but completely de-agglomerated IONPs after  $\sim 10$  min, which could be stabilised (by the carboxyl groups).

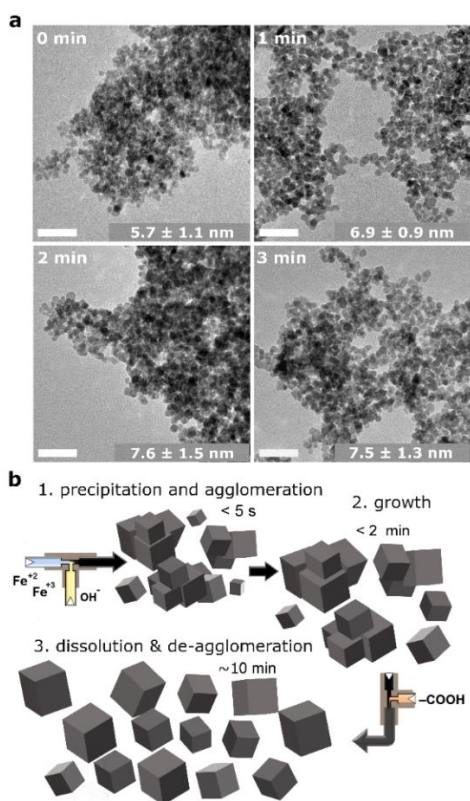


**Figure 8:** (a) TEM images of IONPs obtained using a semi-batch set-up (*i.e.*, sampling from an aging vessel) over time without addition of neutralisation solution (average particle sizes are indicated, the scale bar is 40 nm). The indicated times refer to the time after mixing of the precursor and base solutions. Additional TEM images are shown in Figure S16. (b) Proposed particle formation mechanism during synthesis. 1) Particles are precipitated and agglomerated within seconds, 2) these agglomerated structures continue to grow over the next few minutes till, 3) the addition of the neutralisation solution causes partial dissolution of IONPs and their de-agglomeration over a time scale of  $\sim 10$  min.

## 4. Conclusion

With the aid of flow reactors operated in steady-state mode it became possible to study for the first time, the early stages of co-precipitation syntheses *via* XRD and SAXS (starting from 5 s after mixing the precursor and base solutions). In-situ synchrotron XRD studies revealed that for the synthetic procedure used i) the only crystalline phase present 5 s after mixing was the inverse spinel structure of magnetite/maghemite, ii) the particle size changed only marginally afterwards and solid phase formation (most likely due to particle growth) was completed within two minutes, iii) the mixing conditions showed no effect on the XRD pattern, iv) the presence of dextran during co-precipitation broadened the diffraction peaks significantly indicating smaller coherently scattering domains due to smaller particles. These results differ from previous experimental reports on the initial stages of co-precipitation that showed the occurrence of intermediate phases before the slow (within minutes to hours) transition into magnetite.

The combination of the flow reactor and in-situ SAXS studies showed that just after particle formation, the IONPs were highly agglomerated, indicating that precipitation and agglomeration occur simultaneously. These agglomerates were too large to achieve colloidal stability by simply adding a stabiliser to the precipitated IONP solution, hence, post-processing steps such as ultra-sonication and washing (as standardly used to stabilise co-precipitated IONPs) would be required. As the translation of such post-processing steps into flow is challenging, a novel stabilisation procedure was developed. This was achieved, by adding the right quantity of an acidic solution, e.g., citric acid, after precipitation to neutralise (*i.e.*, reduce the pH value) the IONP solution, and stabilise the IONPs after de-agglomerating the agglomerates formed during co-precipitation. This successful de-agglomeration and stabilisation was shown *via* DLS and time-resolved SAXS studies. The latter revealed that de-agglomeration was achieved within several minutes after the addition of citric acid solution. This proved that this simple and scalable stabilisation procedure is also time efficient making it an effective stabilisation procedure for batch, but especially for flow processes. Furthermore, SAXS analysis showed that the rapid mixing in the flow reactor yielded higher surface to volume ratios than synthesis in batch, indicating the formation of larger agglomerated structures. The particle surface to volume ratio was shown to increase further with improved mixing. However, this increase was marginal, and the mixer chosen for IONP synthesis in flow was a compromise between fast mixing and pressure drop. SQUID magnetometry confirmed that both non-stabilised and stabilised particles were superparamagnetic with considerable mass magnetisation ( $\sim 60 \text{ Am}^2/\text{kg}_{\text{sample}}$ ) for co-precipitated IONPs between 6-7 nm.

The knowledge gained on particle formation and stabilisation kinetics guided the development of a multistage flow reactor for the fully continuous synthesis and stabilisation of superparamagnetic IONPs in aqueous solutions. This multistage flow reactor allowed to perform a co-precipitation synthesis at well-defined temperatures and mixing times below 50 ms, which is hardly achievable in batch systems. The addition of a citric acid solution after the mixing step facilitated de-agglomeration and stabilisation of just-precipitated IONPs in flow, without any intermediate steps. The flow reactor was shown to be robust against fouling and capable of large scale production ( $> 500 \text{ ml/h}$  without parallelisation) yielding reproducibly IONP solutions of remarkable colloidal stability at neutral pH values for costs of chemicals of less than 5 £/g IONPs.

## Acknowledgements

The authors thank the EPSRC U.K. for financial support (EP/M015157/1) through the Manufacturing Advanced Functional Materials (MA-FuMa) scheme. This work was also supported by the CERIC ERIC internal research project: Nano Analytics in Pharmaceuticals. LP was supported by the European Union's Horizon 2020 research and innovation programme under the Marie Skłodowska-Curie grant agreement No 721290. This publication reflects only the author's view, exempting the Community from any liability. Project website: <http://cosmic-etn.eu/>. MMC thanks FCT for financial support under projects UID/MULTI/04046/2019 (BioISI) and PTDC/NAN-MAT/28785/2017. Furthermore, the authors would like to thank Maurizio Polentarutti (Elettra Synchrotron) for his support with the synchrotron XRD studies.

## REFERENCES

1. Fraga-García, P.; Kubbutat, P.; Brammen, M.; Schwaminger, S.; Berensmeier, S. Bare iron oxide nanoparticles for magnetic harvesting of microalgae: from interaction behavior to process realization. *Nanomater.* **2018**, *8*, doi:10.3390/nano8050292.
2. Yuan, J.; Chen, Y.; Li, H.; Lu, J.; Zhao, H.; Liu, M.; Nechitaylo, G.S.; Glushchenko, N.N. New insights into the cellular responses to iron nanoparticles in *Capsicum annuum*. *Sci. Rep.* **2018**, *8*, 3228, doi:10.1038/s41598-017-18055-w.
3. Elmer, W.H.; White, J.C. The use of metallic oxide nanoparticles to enhance growth of tomatoes and eggplants in disease infested soil or soilless medium. *Environ. Sci. Nano* **2016**, *3*, 1072–1079, doi:10.1039/C6EN00146G.
4. Xu, P.; Zeng, G.M.; Huang, D.L.; Feng, C.L.; Hu, S.; Zhao, M.H.; Lai, C.; Wei, Z.; Huang, C.; Xie, G.X.; et al. Use of iron oxide nanomaterials in wastewater treatment: A review. *Sci. Total Environ.* **2012**, *424*, 1–10, doi:10.1016/J.SCITOTENV.2012.02.023.
5. Walker, J.M.; Zaleski, J.M. A simple route to diverse noble metal-decorated iron oxide nanoparticles for catalysis. *Nanoscale* **2016**, *8*, 1535–1544, doi:10.1039/C5NR06700F.
6. Krans, N.A.; van der Feltz, E.C.; Xie, J.; Dugulan, I.A.; Zečević, J.; de Jong, K.P. Attachment of iron oxide nanoparticles to carbon nanotubes and the consequences for catalysis. *ChemCatChem* **2018**, *10*, 3388–3391, doi:10.1002/cctc.201800487.
7. Lin, J.; Raji, A.-R.O.; Nan, K.; Peng, Z.; Yan, Z.; Samuel, E.L.G.; Natelson, D.; Tour, J.M. Iron oxide nanoparticle and graphene nanoribbon composite as an anode material for high-performance Li-ion batteries. *Adv. Funct. Mater.* **2014**, *24*, 2044–2048, doi:10.1002/adfm.201303023.
8. Yuan, H.; Wilks, M.Q.; Normandin, M.D.; El Fakhri, G.; Kaittanis, C.; Josephson, L. Heat-induced radiolabeling and fluorescence labeling of feraheme nanoparticles for PET/SPECT imaging and flow cytometry. *Nat. Protoc.* **2018**, *13*, 392–412, doi:10.1038/nprot.2017.133.
9. Ling, D.; Lee, N.; Hyeon, T. Chemical synthesis and assembly of uniformly sized iron oxide nanoparticles for medical

- applications. *Acc. Chem. Res.* **2015**, *48*, 1276–1285, doi:10.1021/acs.accounts.5b00038.
10. Espinosa, A.; Di Corato, R.; Kolosnjaj-Tabi, J.; Flaud, P.; Pellegrino, T.; Wilhelm, C. Duality of Iron Oxide nanoparticles in cancer therapy: amplification of heating efficiency by magnetic hyperthermia and photothermal bimodal treatment. *ACS Nano* **2016**, *10*, 2436–2446, doi:10.1021/acs.nano.5b07249.
  11. Hola, K.; Markova, Z.; Zoppellaro, G.; Tucek, J.; Zboril, R. Tailored functionalization of iron oxide nanoparticles for MRI, drug delivery, magnetic separation and immobilization of biosubstances. *Biotechnol. Adv.* **2015**, *33*, 1162–1176, doi:10.1016/J.BIOTECHADV.2015.02.003.
  12. El-Boubbou, K. Magnetic iron oxide nanoparticles as drug carriers: preparation, conjugation and delivery. *Nanomedicine* **2018**, *13*, 929–952, doi:10.2217/nnm-2017-0320.
  13. Laurent, S.; Saei, A.A.; Behzadi, S.; Panahifar, A.; Mahmoudi, M. Superparamagnetic iron oxide nanoparticles for delivery of therapeutic agents: opportunities and challenges. *Expert Opin. Drug Deliv.* **2014**, *11*, 1449–1470, doi:10.1517/17425247.2014.924501.
  14. Martinez-Boubeta, C.; Simeonidis, K.; Makridis, A.; Angelakeris, M.; Iglesias, O.; Guardia, P.; Cabot, A.; Yedra, L.; Estradé, S.; Peiró, F.; et al. Learning from nature to improve the heat generation of iron-oxide nanoparticles for magnetic hyperthermia applications. *Sci. Rep.* **2013**, *3*, 1652, doi:10.1038/srep01652.
  15. Alves, A.F.; Mendo, S.G.; Ferreira, L.P.; Mendonça, M.H.; Ferreira, P.; Godinho, M.; Cruz, M.M.; Carvalho, M.D. Gelatine-assisted synthesis of magnetite nanoparticles for magnetic hyperthermia. *J. Nanoparticle Res.* **2016**, *18*, 1–13, doi:10.1007/s11051-016-3327-z.
  16. Bao, Y.; Sherwood, J.A.; Sun, Z. Magnetic iron oxide nanoparticles as  $T_1$  contrast agents for magnetic resonance imaging. *J. Mater. Chem. C* **2018**, *6*, 1280–1290, doi:10.1039/C7TC05854C.
  17. Hachani, R.; Lowdell, M.; Birchall, M.; Hervault, A.; Mertz, D.; Begin-Colin, S.; Thanh, N.T.K. Polyol synthesis, functionalisation, and biocompatibility studies of superparamagnetic iron oxide nanoparticles as potential MRI contrast agents. *Nanoscale* **2016**, *8*, 3278–3287, doi:10.1039/C5NR03867G.
  18. Laurent, S.; Forge, D.; Port, M.; Roch, A.; Robic, C.; Vander Elst, L.; Muller, R.N. Magnetic iron oxide nanoparticles: synthesis, stabilization, vectorization, physicochemical characterizations, and biological applications. *Chem. Rev.* **2008**, *108*, 2064–2110, doi:10.1021/cr068445e.
  19. Gupta, A.K.; Gupta, M. Synthesis and surface engineering of iron oxide nanoparticles for biomedical applications. *Biomaterials* **2005**, *26*, 3995–4021, doi:10.1016/J.BIOMATERIALS.2004.10.012.
  20. Wu, W.; Wu, Z.; Yu, T.; Jiang, C.; Kim, W.-S. Recent progress on magnetic iron oxide nanoparticles: synthesis, surface

- functional strategies and biomedical applications. *Sci. Technol. Adv. Mater.* **2015**, *16*, 023501, doi:10.1088/1468-6996/16/2/023501.
21. Sun, S.; Zeng, H. Size-controlled synthesis of magnetite nanoparticles. *J. Am. Chem. Soc.* **2002**, *124*, 8204–8205, doi:10.1021/JA026501X.
  22. Chen, C.-J.; Lai, H.-Y.; Lin, C.-C.; Wang, J.-S.; Chiang, R.-K. Preparation of monodisperse iron oxide nanoparticles via the synthesis and decomposition of iron fatty acid complexes. *Nanoscale Res. Lett.* **2009**, *4*, 1343–50, doi:10.1007/s11671-009-9403-x.
  23. Hyeon, T.; Lee, S.S.; Park, J.; Chung, Y.; Na, H.B. Synthesis of highly crystalline and monodisperse maghemite nanocrystallites without a size-selection process. *J. Am. Chem. Soc.* **2001**, *123*, 12798–801.
  24. Kim, B.H.; Lee, N.; Kim, H.; An, K.; Park, Y. II; Choi, Y.; Shin, K.; Lee, Y.; Kwon, S.G.; Na, H. Bin; et al. Large-scale synthesis of uniform and extremely small-sized iron oxide nanoparticles for high-resolution T-1 magnetic resonance imaging contrast agents. *J. Am. Chem. Soc.* **2011**, *133*, 12624–12631, doi:10.1021/ja203340u.
  25. Kwon, S.G.; Piao, Y.; Park, J.; Angappane, S.; Jo, Y.; Hwang, N.-M.; Park, J.-G.; Hyeon, T. Kinetics of monodisperse iron oxide nanocrystal formation by “heating-up” process. *J. Am. Chem. Soc.* **2007**, *129*, 12571–12584, doi:10.1021/ja074633q.
  26. Lassenberger, A.; Grünewald, T.A.; van Oostrum, P.D.J.; Rennhofer, H.; Amenitsch, H.; Zirbs, R.; Lichtenegger, H.C.; Reimhult, E. Monodisperse iron oxide nanoparticles by thermal decomposition: elucidating particle formation by second-resolved in situ Small-Angle X-ray Scattering. *Chem. Mater.* **2017**, *29*, 4511–4522, doi:10.1021/acs.chemmater.7b01207.
  27. Grabs, I.-M.; Bradtmöller, C.; Menzel, D.; Garnweitner, G. Formation mechanisms of iron oxide nanoparticles in different nonaqueous media. *Cryst. Growth Des.* **2012**, *12*, 1469–1475, doi:10.1021/cg201563h.
  28. Ahn, T.; Kim, J.H.; Yang, H.-M.; Lee, J.W.; Kim, J.-D. Formation pathways of magnetite nanoparticles by coprecipitation method. *J. Phys. Chem. C* **2012**, *116*, 6069–6076, doi:10.1021/jp211843g.
  29. Baumgartner, J.; Dey, A.; Bomans, P.H.H.; Le Coadou, C.; Fratzl, P.; Sommerdijk, N.A.J.M.; Faivre, D. Nucleation and growth of magnetite from solution. *Nat. Mater.* **2013**, *12*, 310–314, doi:10.1038/nmat3558.
  30. Jolivet, J.-P.; Chanéac, C.; Tronc, E. Iron oxide chemistry. From molecular clusters to extended solid networks. *Chem. Commun.* **2004**, *54*, 477–483, doi:10.1039/B304532N.
  31. Jolivet, J.-P.; Henry, M.; Livage, J. *Metal Oxide Chemistry and Synthesis: from Solution to Solid State*; John Wiley: New York, 2000; ISBN 9780471970569.

32. Scheck, J.; Wu, B.; Drechsler, M.; Rosenberg, R.; Van Driessche, A.E.S.; Stawski, T.M.; Gebauer, D. The molecular mechanism of iron(III) oxide nucleation. *J. Phys. Chem. Lett.* **2016**, *7*, 3123–3130, doi:10.1021/acs.jpcllett.6b01237.
33. Sun, S.; Gebauer, D.; Cölfen, H. Alignment of amorphous iron oxide clusters: a non-classical mechanism for magnetite formation. *Angew. Chemie Int. Ed.* **2017**, *56*, 4042–4046, doi:10.1002/anie.201610275.
34. Blanco-Andujar, C.; Ortega, D.; Pankhurst, Q.A.; Thanh, N.T.K. Elucidating the morphological and structural evolution of iron oxide nanoparticles formed by sodium carbonate in aqueous medium. *J. Mater. Chem.* **2012**, *22*, 12498, doi:10.1039/c2jm31295f.
35. LaGrow, A.P.; Besenhard, M.O.; Hodzic, A.; Sergides, A.; Bogart, L.K.; Gavriilidis, A.; Thanh, N.T.K. Unravelling the growth mechanism of the co-precipitation of iron oxide nanoparticles with the aid of synchrotron X-Ray diffraction in solution. *Nanoscale* **2019**, *11*, 6620–6628, doi:10.1039/C9NR00531E.
36. Haseidl, F.; Müller, B.; Hinrichsen, O. Continuous-flow synthesis and functionalization of magnetite: intensified process for tailored nanoparticles. *Chem. Eng. Technol.* **2016**, *39*, 2051–2058, doi:10.1002/ceat.201600163.
37. Lim, J.-M.; Swami, A.; Gilson, L.M.; Chopra, S.; Choi, S.; Wu, J.; Langer, R.; Karnik, R.; Farokhzad, O.C. Ultra-high throughput synthesis of nanoparticles with homogeneous size distribution using a coaxial turbulent jet mixer. *ACS Nano* **2014**, *8*, 6056–6065, doi:10.1021/nn501371n.
38. Li, T.; Senesi, A.J.; Lee, B. Small Angle X-ray Scattering for nanoparticle research. *Chem. Rev.* **2016**, *116*, 11128–11180, doi:10.1021/acs.chemrev.5b00690.
39. Girod, M.; Vogel, S.; Szczerba, W.; Thünemann, A.F. How temperature determines formation of maghemite nanoparticles. *J. Magn. Magn. Mater.* **2015**, *380*, 163–167, doi:10.1016/j.jmmm.2014.09.057.
40. LaGrow, A.P.; Besong, T.M.D.; AlYami, N.M.; Katsiev, K.; Anjum, D.H.; Abdelkader, A.; Costa, P.M.F.J.; Burlakov, V.M.; Goriely, A.; Bakr, O.M. Trapping shape-controlled nanoparticle nucleation and growth stages via continuous-flow chemistry. *Chem. Commun.* **2017**, *53*, 2495 – 2498, doi:10.1039/C6CC08369B.
41. Frenz, L.; El Harrak, A.; Pauly, M.; Bégin-Colin, S.; Griffiths, A.D.; Baret, J.-C. Droplet-based microreactors for the synthesis of magnetic iron oxide nanoparticles. *Angew. Chemie Int. Ed.* **2008**, *47*, 6817–6820, doi:10.1002/anie.200801360.
42. Kumar, K.; Nightingale, A.M.; Krishnadasan, S.H.; Kamaly, N.; Wylenzinska-Arridge, M.; Zeissler, K.; Branford, W.R.; Ware, E.; deMello, A.J.; deMello, J.C. Direct synthesis of dextran-coated superparamagnetic iron oxide nanoparticles in a capillary-based droplet reactor. *J. Mater. Chem.* **2012**, *22*, 4704, doi:10.1039/c2jm30257h.
43. Larrea, A.; Sebastian, V.; Ibarra, A.; Arruebo, M.; Santamaria, J. Gas slug microfluidics: a unique tool for ultrafast,

- highly controlled growth of iron oxide nanostructures. *Chem. Mater.* **2015**, *27*, 4254–4260, doi:10.1021/acs.chemmater.5b00284.
44. Simmons, M.; Wiles, C.; Rocher, V.; Francesconi, M.G.; Watts, P. The preparation of magnetic iron oxide nanoparticles in microreactors. *J. Flow Chem.* **2013**, *3*, 7–10, doi:10.1556/JFC-D-12-00024.
45. Besenhard, M.O.; Neugebauer, P.; Scheibelhofer, O.; Khinast, J.G. Crystal engineering in continuous plug-flow crystallizers. *Cryst. Growth Des.* **2017**, *17*, 6432–6444, doi:10.1021/acs.cgd.7b01096.
46. Lee, K.M.; Kim, S.-G.; Kim, W.-S.; Kim, S.S. Properties of iron oxide particles prepared in the presence of dextran. *Korean J. Chem. Eng.* **2002**, *19*, 480–485, doi:10.1007/BF02697160.
47. Osborne, E.A.; Atkins, T.M.; Gilbert, D.A.; Kauzlarich, S.M.; Liu, K.; Louie, A.Y. Rapid microwave-assisted synthesis of dextran-coated iron oxide nanoparticles for magnetic resonance imaging. *Nanotechnology* **2012**, *23*, 215602, doi:10.1088/0957-4484/23/21/215602.
48. Szczerba, W.; Costo, R.; Veintemillas-Verdaguer, S.; Del Puerto Morales, M.; Thünemann, A.F. SAXS analysis of single-and multi-core iron oxide magnetic nanoparticles. *J. Appl. Crystallogr.* **2017**, *50*, 481–488, doi:10.1107/S1600576717002370.
49. Bang, J.H.; Suslick, K.S. Applications of ultrasound to the synthesis of nanostructured materials. *Adv. Mater.* **2010**, *22*, 1039–1059, doi:10.1002/adma.200904093.
50. Gentile, L.; Wang, T.; Tunlid, A.; Olsson, U.; Persson, P. Ferrihydrite nanoparticle aggregation induced by dissolved organic matter. *J. Phys. Chem. A* **2018**, *122*, 7730–7738, doi:10.1021/ACS.JPCA.8B05622.
51. Uson, L.; Arruebo, M.; Sebastian, V.; Santamaria, J. Single phase microreactor for the continuous, high-temperature synthesis of < 4 nm superparamagnetic iron oxide nanoparticles. *Chem. Eng. J.* **2018**, *340*, 66–72, doi:10.1016/J.CEJ.2017.12.024.
52. Huang, H.; Du Toit, H.; Besenhard, M.O.; Ben-Jaber, S.; Dobson, P.; Parkin, I.; Gavriilidis, A. Continuous flow synthesis of ultrasmall gold nanoparticles in a microreactor using trisodium citrate and their SERS performance. *Chem. Eng. Sci.* **2018**, *198*, 422–430, doi:10.1016/j.ces.2018.06.050.